Oxygen Activation by Rieske Non-Heme Iron Oxygenases, a Theoretical Insight

ARTICLE *in* THE JOURNAL OF PHYSICAL CHEMISTRY B · AUGUST 2004

Impact Factor: 3.3 · DOI: 10.1021/jp048515q

4 AUTHORS, INCLUDING:

Tomasz Borowski
Instytut Katalizy i Fizykochemii Powierzchni i…
45 PUBLICATIONS **1,208** CITATIONS

Oxygen Activation by Rieske Non-Heme Iron Oxygenases, a Theoretical Insight

Arianna Bassan,* Margareta R. A. Blomberg, Tomasz Borowski, and Per E. M. Siegbahn

Department of Physics, Stockholm University, SE 106 91 Stockholm, Sweden

Received: April 5, 2004; In Final Form: June 18, 2004

The first steps of dioxygen activation in naphthalene 1,2-dioxygenase have been investigated by means of hybrid density functional theory. Reduction of molecular oxygen by this Rieske dioxygenase occurs in the catalytic domain accommodating a mononuclear non-heme iron(II) complex, and it requires two external electrons ultimately delivered by a Rieske [2Fe−2S] cluster hosted in the neighboring domain. Theoretical tools have been applied to gain insight into the O_2-binding step and into the first one-electron-transfer process involving the mononuclear and the Rieske centers, and yielding an iron(II)−superoxo intermediate. The reaction, which is mimicked with a model including both metal sites, is found to be a reversible equilibrium. Although the entropic loss associated with the binding of O_2 to iron(II) is not canceled by the corresponding enthalpic binding energy, it is, however, balanced by the exothermicity of the electron transfer process from the Rieske cluster to the dioxygen-bound iron(II) complex. The rationalization for the calculated energetics is related to the values of the ionization potential (IP) of the Rieske cluster and the electron affinity (EA) of the mononuclear iron complex: the latter is computed to be higher than the former, when dioxygen is bound to the metal. The possibility that a second external electron is delivered to the mononuclear site before dioxygenation of the substrate has also been examined. It is shown that, if the second electron is available in the Rieske domain, the electron transfer process is energetically favored. The results acquired with the large model comprising the two metal centers are compared to the corresponding information collected from the study of smaller models, where either the mononuclear iron complex or the Rieske cluster is included.

1. Introduction

Aromatic hydrocarbons are serious environmental pollutants that can be degraded by bacteria under aerobic conditions. The catabolic pathway for the degradation of these compounds is usually initiated by bacterial Rieske non-heme iron dioxygenases, which catalyze the *cis*-dihydroxylation reaction of an aromatic ring, yielding the corresponding *cis*-diol.[1]

Naphthalene 1,2-dioxygenase, which is one of the best studied Rieske dioxygenases, uses molecular oxygen to oxidize naphthalene in a stereospecific manner to *cis*-(1*R*,2*S*)-dihydroxy-1,2-dihydronaphthalene, where both oxygen atoms originate from O_2.[2] Two of the four electrons required to reduce molecular oxygen are provided by the aromatic substrate and the remaining two electrons are supplied by an external source, the reduced form of nicotinamide adenine nucleotide (NADH). As shown in Figure 1, the two external electrons are transferred one at a time through the three components of the enzyme: (a) a flavoprotein reductase containing an iron−sulfur cluster; (b) a Rieske [2Fe−2S] ferredoxin; (c) an oxygenase component accommodating a Rieske [2Fe−2S] cluster and a mononuclear iron(II) center. NADH binds in the reductase component and molecular oxygen oxidizes naphthalene in the oxygenase component.[3−8]

The oxygenase component is an $\alpha_3\beta_3$ hexamer.[3] It is believed that the β-subunit has a mere structural role. Naphthalene dioxygenation occurs in the α subunit, and specifically in the catalytic domain where the mononuclear iron(II) site is located (see Figure 2). The metal ion in the catalytic domain is coordinated by the 2-His-1-carboxylate facial triad,[9,10] a common motif in many non-heme iron enzymes involved in a wide variety of biological processes.[11−13] In the resting state of the

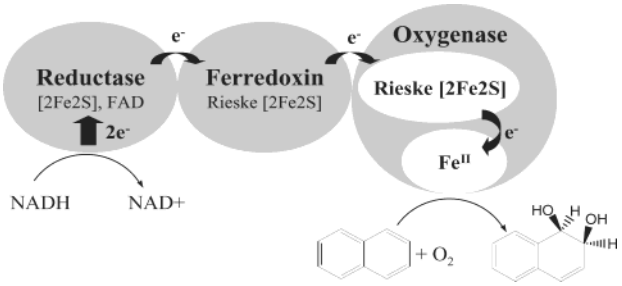

Figure 1. Electron-transfer path in the multicomponent enzyme naphthalene 1,2-dioxygenase.

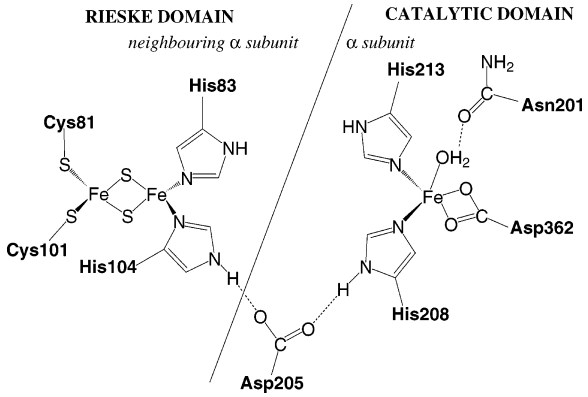

Figure 2. Two metal centers in the oxygenase component of naphthalene 1,2-dioxygenase. Substrate oxidation occurs in the catalytic domain, whereas the Rieske cluster mediates electron transfers. The two metal complexes are linked by Asp205.

* To whom correspondence should be addressed. Telephone: +46 8 55378707. Fax: +46 8 55378601. E-mail: arianna@physto.se.

10.1021/jp048515q CCC: $27.50
Published on Web 08/04/2004

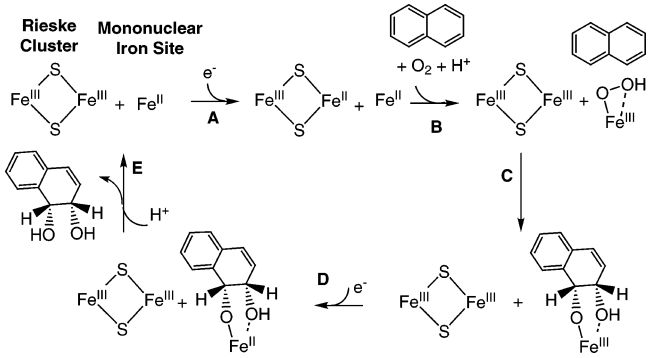

Figure 3. Proposed mechanism of aromatic *cis*-dihydroxylation passing through a ferric-hydroperoxo intermediate.

enzyme, the coordination of iron can be viewed as a distorted octahedral with a missing ligand; the first coordination sphere of the metal is occupied by two histidines (His208 and His213), a bidentate aspartate (Asp362), and a water molecule. Recent crystallographic data of naphthalene dioxygenase show dioxygen trapped in the catalytic domain; dioxygen was detected to bind side-on to the metal after the displacement of the water ligand.[7,14] The α subunit also contains a second domain (Rieske domain) hosting a Rieske [2Fe−2S] cluster, which includes two iron atoms, one coordinated by two cysteines (Cys101 and Cys81) and one coordinated by two histidines (His83 and His104). In the resting state of the enzyme, the Rieske cluster is oxidized, having both iron atoms in the ferric form. It becomes reduced during catalysis while mediating the one-electron transfer from the ferredoxin component to the catalytic domain (Figure 1). In the reduced state the extra electron reduces the iron atom coordinated by the two histidines.[15] The Rieske cluster is connected through an aspartate residue (Asp205) to the mononuclear iron complex belonging to a neighboring α subunit, as illustrated in Figure 2. The Rieske and the mononuclear centers located in the same subunit instead are more than 40 Å apart.

The mechanism that accounts for dioxygen activation in naphthalene dioxygenase is still under debate. Convincingly, the conclusions drawn from the single turnover experiments by Lipscomb and co-workers suggest that dioxygen is activated via reduction by one external electron, yielding a iron(III)−(hydro)peroxo intermediate (Figure 3).[16,17] It was observed that in the absence of the reductase and the ferredoxin components, the oxygenase component was still capable of naphthalene dihydroxylation if the Rieske cluster was in the reduced form (i.e., reduced by one electron) and the mononuclear iron center was in the ferrous state. During single turnover, the mononuclear iron site was oxidized to the ferric form and consequently two electrons, one from the reduced Rieske cluster and one from the mononuclear iron(II) complex were sufficient to initiate dioxygen activation and thus to perform naphthalene dioxygenation.[16] Interestingly, the "peroxide shunt" (i.e., hydrogen peroxide is used as oxidant instead of molecular oxygen) with the Rieske cluster in the oxidized state also yields the diol.[17] The formation of a (hydro)peroxo species along the reaction pathway is supported by the uncoupling of dioxygen reduction and substrate dihydroxylation observed with benzene as substrate; in this case release of hydrogen peroxide was detected.[18]

The different experimental observations on the activity of naphthalene dioxygenase suggest the catalytic cycle sketched in Figure 3. The oxidized Rieske cluster is initially reduced by one external electron (step A), which is then transferred to the mononuclear iron center when dioxygen and naphthalene bind to the active site (step B). The so-formed ferric-(hydro)peroxo intermediate reacts with the substrate, yielding the diol and a ferric complex (step C). The initial ferrous oxidation state of the mononuclear iron site is finally regenerated by the transfer of a second external electron (steps D and E). In principle, the second electron may enter the cycle even before substrate dioxygenation, yielding a ferrous-(hydro)peroxo species. However, the single turnover experiments by Lipscomb and co-workers show that this is not necessary for substrate hydroxylation.[16,17]

Naphthalene dioxygenation by the ferric-(hydro)peroxide may involve the formation of a high-valent iron oxo species (OH−Fe^{V}═O) produced by initial O−O bond lysis. Alternatively, the peroxide may directly attack the substrate. Very recently, we investigated by means of theoretical tools how the ferric-hydroperoxo species carries out naphthalene dihydroxylation and, on the basis of the computed energetics, we proposed a mechanism passing through an epoxide intermediate, which subsequently decays into the diol.[19] The involvement of the high-valent iron-oxo species was dismissed because of too high an activation barrier associated with the O−O bond cleavage.

In the present study, quantum chemical methods are used to explore the first steps of dioxygen activation leading to the formation of the ferric-(hydro)peroxo species (steps A and B of Figure 3). The properties of the Rieske iron−sulfur cluster and the mononuclear iron center are investigated in relation to the electron-transfer process. The possibility that a second external electron is supplied to the catalytic domain before substrate dihydroxylation yielding a ferrous-hydroperoxo intermediate, has also been investigated.

2. Computational Details

Hybrid density functional theory with the B3LYP functional[20,21,22] has been employed to study dioxygen activation in naphthalene dioxygenase. All the systems investigated were characterized by an open-shell electronic configuration and thus unrestricted DFT was used. Optimized geometries and corresponding energies were obtained with the two quantum chemical programs Jaguar 4.2[23] and Gaussian 98.[24]

An effective core potential was used to describe iron.[25] Following a well tested computational procedure,[26,27] in the geometry optimizations all the other atoms were described by a standard double-ζ basis set, which is labeled lacvp in Jaguar. The final B3LYP energies for the fully optimized structures were computed using a larger basis set with polarization functions on all atoms (labeled lacv3p** in Jaguar[23]). Spin populations obtained with the smaller basis set are reported. A few geometries were also optimized with a double-ζ basis set including polarization functions (lacvp**) and the energy differences of interest were compared to the ones obtained from the standard approach.

To reproduce the polarization effects of the protein, the self-consistent reaction field as implemented in Jaguar was employed.[28,29] The solvent is modeled as a macroscopic continuum with a low dielectric constant ($\epsilon = 4.0$) and the solute as placed in a cavity contained in this continuous medium. The probe radius was chosen to be 1.4 Å. The correction due to the solvent effects was determined by employing the lacvp basis set. In general, the dielectric does not significantly affect the computed energetics, except when charge-transfer processes are examined, where solvent effects play a crucial role for the evaluation of electron affinities and ionization potentials.

The low-spin ("broken symmetry") ground state obtained from the antiferromagnetic spin coupling of the high-spin states in the Rieske cluster, is heavily spin contaminated. The correction to the "broken symmetry" state of the reduced and

the oxidized state is estimated from the Heisenberg spin coupling (J_{ox} and J_{red}).[30] In the case of J_{red} the resonance delocalization parameter (B) was neglected. In summary, the complete expression for the ionization potential (IP) is

$$\mathrm{IP} = \mathrm{IP}_g + \Delta s + \Delta z + \Delta\mathrm{BS} \quad (1)$$

where IP_g is the computed IP in the gas phase, Δs the correction due to the dielectric effects ($\epsilon = 4$), Δz is the correction due to the zero-point effects, and ΔBS is the correction obtained from the evaluation of J_{ox} and J_{red}. An analogous expression defines the electron affinity (EA). It should be noted that an accurate evaluation of IPs and EAs is not an easy task and may require a more detailed inclusion of the effects exerted by the protein environment on the electron donor or electron acceptor.

The rigidity of the protein backbone is reproduced in the theoretical modeling by freezing some positions of the cluster according to the available X-ray data. This procedure turns out to be useful especially when the model contains residues not anchored in the first coordination sphere of a metal.[31] Because the frozen coordinates preclude an accurate derivation of the Gibbs free energy and because zero-point and thermal effects are expected to be small for the energy differences of interest (ionization potentials and electron affinities), molecular Hessians were in general not calculated. Only in a few cases were second derivatives evaluated, and zero-point and/or thermal effects derived. In these particular cases, the corrections made to the computed energy differences are specified.

The accuracy of the B3LYP functional can be obtained from the benchmark tests performed on a wide array of molecules (radicals, non-hydrogen systems, hydrocarbons, substituted hydrocarbons and inorganic hydrides)[32] and transition metal systems.[27,33,34] Test calculations aimed at evaluating the binding energy of O_2 to Fe^{II} were performed using two methods: the B3LYP functional and the CCSD(T) level of theory. More specifically, geometries were optimized with a standard double-ζ basis set (i.e., the lacvp basis set) and final energies were obtained with the lacv3p** basis set for the B3LYP case and the 6-311+G(2d,2p) basis set for the CCSD(T) case. The computed binding energies of O_2 derived from these calculations with an $[Fe^{II}(OH)_2]$ model show that the two methods predict almost identical binding energies (the two computed binding energies are 11.5 and 12.0 kcal/mol for the B3LYP and CCSD(T) methods, respectively). From the available benchmark calculations, it can be concluded that an error of about 3−5 kcal/mol could affect the relative computed energies.

The rate of electron transfer (ET) between the Rieske cluster and the mononuclear site was estimated using semiclassical Marcus theory.[35] In this approach, the rate constant k_{ET} for the ET reaction depends on the driving force ΔG of the process, the reorganization energy λ, and the donor−acceptor electronic coupling matrix element H_{DA}. In the isotropic model, the contribution of H_{DA} to k_{ET} is expressed by an exponential function depending on the distance d between the sites and on a scalable parameter β:

$$k_{ET} = 10^{13} \exp(-d\beta) \exp[-(\Delta G + \lambda)^2/4\lambda RT] \quad (2)$$

The activation energy for the ET process is defined as

$$E_a = \frac{(\Delta G + \lambda)^2}{4\lambda} \quad (3)$$

In the calculations reported here, the distance d between the sites was obtained from the iron−iron separation minus 3 Å to account for the van der Waal's contact.[36,37] The reorganization energy λ is defined as the energy needed to distort the products (reactants) into the configuration of the reactants (products). The reorganization energy can be further divided into the internal reorganization energy of the molecules exchanging the electron (λ_i) and the solvent contribution (λ_{solv}):

$$\lambda = \lambda_i + \lambda_{solv} \quad (4)$$

In the current study, the energy of the oxidized state in the optimal geometry of the reduced state and the energy of the reduced state in the optimal geometry of the oxidized state were used to derive the reorganization energy (dielectric effects were included to partially account for λ_{solv}). The simple tight-binding Hamiltonian model, developed for proteins by Beratan and Onuchic to calculate the β parameter, was employed.[36,38,39] In this approach, the coupling matrix element for a given ET pathway is proportional to the product of the decay factors for covalent bonds (ϵ_C), hydrogen bonds (ϵ_H) and space jumps ϵ_S

$$H_{DA} \propto \prod \epsilon_C \prod \epsilon_H \prod \epsilon_S \quad (5)$$

The decay factor for covalent bonds and regular hydrogen bonds (with separation below 2.1 Å) is 0.6. Factors for space jumps and longer hydrogen bonds decay exponentially with the distance:

$$\epsilon_S = 0.6 \exp[-1.7(R - 1.4)] \quad (6)$$

$$\epsilon_H = 0.6 \exp[-1.7(R - 2.1)] \qquad R > 2.1\ \text{Å} \quad (7)$$

The contribution of the metal d-orbitals to the H_{DA} value was set equal to 1.

3. Results and Discussion

Dioxygen activation yielding the ferric-hydroperoxo species in the oxygenase component of the Rieske-type naphthalene dioxygenase has been investigated by means of theoretical tools. As shown in Figure 3 (steps A and B), the formation of the ferric intermediate implicates three processes: (a) dioxygen binding to the mononuclear iron(II) complex; (b) electron transfer from the external source NADH (the Rieske cluster in the Rieske domain mediates this electron transfer); (c) proton transfer. The effects of the substrate binding in the active site cannot be reproduced by the present modeling, and they are considered to play a negligible role on the energetics of the process studied.

To shed light on these chemical events, the ionization potential (IP) of the Rieske cluster is computed; the energy $\Delta E(O_2)$ of the binding of molecular oxygen to iron(II) is also evaluated together with the electron affinity (EA) of the $[Fe^{II}-O_2]^{2+}$ complex according to the following expressions:

$$\mathrm{Rieske}_{red} \rightarrow \mathrm{Rieske}_{ox} + e^-$$
$$\mathrm{IP} = E(\mathrm{Rieske}_{ox}) - E(\mathrm{Rieske}_{red}) \quad (8)$$

$$Fe^{2+} + O_2 \rightarrow [Fe^{II}-O_2]^{2+}$$
$$\Delta E(O_2) = E([Fe^{II}-O_2]^{2+}) - E(Fe^{2+}) - E(O_2) \quad (9)$$

$$[Fe^{II}-O_2]^{2+} + e^- \rightarrow [Fe^{II}-O_2]^{+}$$
$$\mathrm{EA} = E([Fe^{II}-O_2]^{2+}) - E([Fe^{II}-O_2]^{+}) \quad (10)$$

Evaluation of the IP/EA values provides useful insight into the

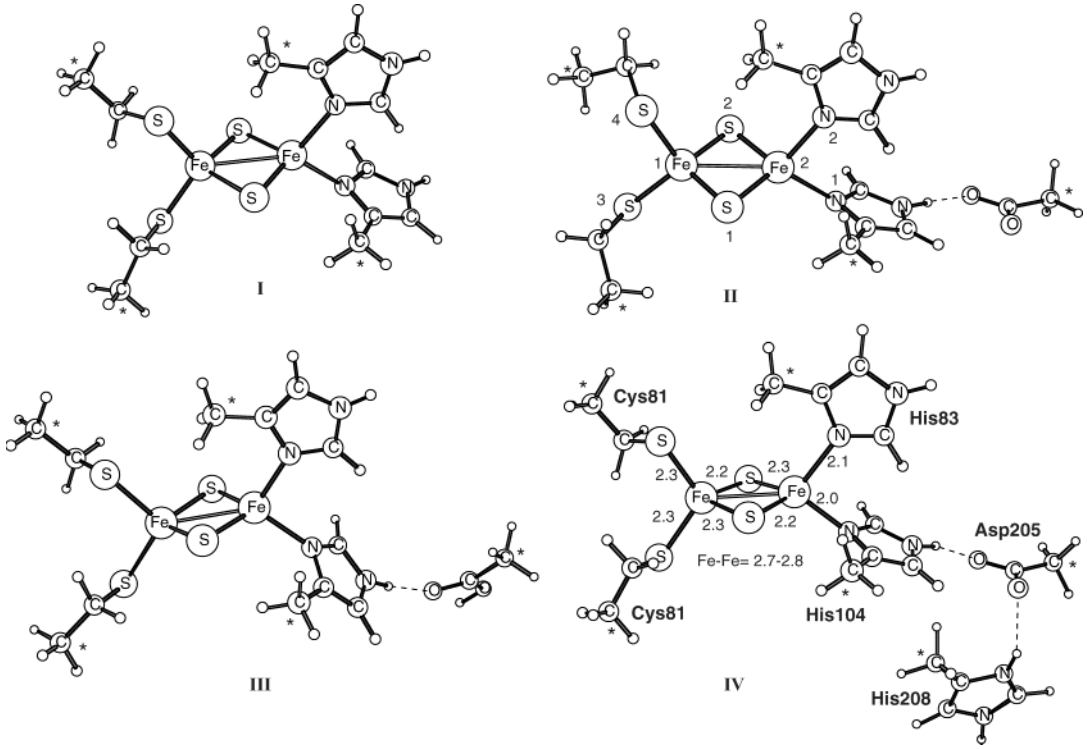

Figure 4. Four models for the Rieske cluster. The smallest model, I, includes only the metal first coordination sphere; in the other models, residues located in the outer coordination spheres are added. I, III, and IV are neutral in the oxidized state, whereas II is negatively charged. Atoms marked with an asterisk were frozen during geometry optimizations. The labeling of the atoms is shown in II. Structure IV reports distances (Å) as derived from the X-ray data of refs 7 and 14.

electron transfer processes involving the two metal centers. More specifically, the relative values of the IP and the EA govern the energetics associated with the electron transfer between the Rieske and the catalytic domains. Lack of experimental information on the actual hydrogen bonding network supplying protons (i.e., on the protonated residues delivering the protons) to the active site, hampers a detailed theoretical investigation of the third step, namely, the proton transfer leading to the iron(III)-hydroperoxo species.

A second external electron is available from NADH and it was suggested that it is delivered to the mononuclear site after substrate dioxygenation (step D, Figure 3). To study if the second external electron may reach the mononuclear iron center at an earlier stage of catalysis, namely, right after the formation of the iron(III)-hydroperoxo intermediate, the EA of $[Fe^{III}-OOH]^{2+}$ was evaluated according to the following scheme:

$$[Fe^{III}-OOH]^{2+} + e^- \rightarrow [Fe^{II}-OOH]^{+}$$
$$EA = E([Fe^{III}-OOH]^{2+}) - E([Fe^{II}-OOH]^{+}) \quad (11)$$

The dioxygen activation process was investigated with a large model comprising both the mononuclear non-heme iron complex and the iron−sulfur cluster of the oxygenase component sketched in Figure 2. Hence, the electron transfer occurring in the dioxygen activation process (step A of Figure 3) has been explored including both the electron donor (i.e., the reduced Rieske cluster) and the electron acceptor (i.e., the mononuclear non-heme iron site) in the model. Because the two metal centers are separated by a relatively short distance (∼12 Å), the resulting model was still affordable by a quantum chemical approach. Nevertheless, smaller models comprising either the Rieske cluster or the mononuclear iron(II) complex have also been examined, providing more detailed information on the various chemical properties of the two metal sites. Furthermore, a comparison among different modeling approaches is useful to discern potential computational artifacts. The results from the largest model are considered to be the most accurate of the present study.

In the models of the Rieske cluster, the cysteine ligands (Cys81 and Cys101 of Figure 2) are included as ethanethiolates, whereas the histidine ligands in both the Rieske cluster and in the mononuclear complex are modeled as 4-methylimidazoles. An acetate is chosen to replace aspartate Asp362 belonging to the 2-His-1-carboxylate motif and the aspartate residue Asp205 joining the two metal centers. Finally, Asn201 is also included in some structures in the form of acetylamide. The rigidity of the protein backbone is reproduced, constraining some coordinates according to the available X-ray data.[7,14]

Because NO is often used in place of O_2 to gain structural insights into the enzyme active site and because EPR spectroscopy[16] and X-ray data[7] show that a nitrosyl adduct can be formed in naphthalene dioxygenase, the binding of NO to the mononuclear iron(II) site is examined and compared to the binding of O_2. The possibility of one-electron transfer from the neighboring reduced Rieske cluster is also considered.

3.1. Rieske Cluster. The ionization potential of the Rieske cluster was calculated by employing the different models shown in Figure 4 (the labeling for the different atoms is shown). The four models mainly differ in size and total charge. Models I, III, and IV are neutral in the oxidized state, and negatively charged when reduced; model II has instead charge −1 in the oxidized state. The model was further extended to the mononuclear iron(II) complex obtaining system V shown in Figure 5.

The oxidized state of all models includes the two iron ions in the formal ferric oxidation state; in the reduced cluster, the iron ion ligated by the two histidines has the lower formal oxidation state (Fe^{II}).[15] In agreement with previous experiments

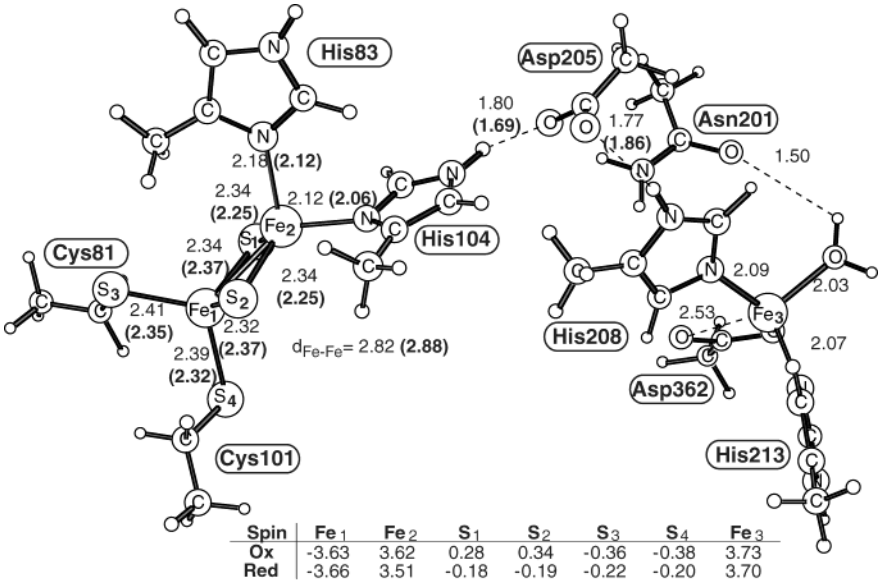

Figure 5. Big model for the Rieske cluster, including the mononuclear iron(II) center. Bond distances (Å) of the reduced cluster are shown together with those of the oxidized cluster (in parentheses). The corresponding spin distributions are reported.

TABLE 1: Relevant Bond Distances and Spin Populations As Determined for the Small Model I of the Oxidized and Reduced Rieske Clusters with Antiferromagnetic Coupling

	distance to Fe1 (Å)			distance to Fe2 (Å)		spin				
	Fe2	S1 S2	S3 S4	N1 N1	S1 S2	Fe1	Fe2	S1 S2	S3 S3	IP[b] (kcal mol^{-1})
Rieske$_{ox}$	2.86	2.38	2.32	2.07	2.25	−3.63	3.60	0.30	−0.39	
($S = 0$)		2.37	2.34	2.08	2.25			0.37	−0.37	
Rieske$_{red}$	2.76	2.34	2.38	2.09	2.35	−3.68	3.51	−0.21	−0.26	82.4
($S = 1/2$)		2.34	2.42	2.16	2.32			−0.17	−0.24	
Rieske$_{ox}$[a]	2.82	2.33	2.31	2.12	2.21					
($S = 0$)		2.34	2.29	2.11	2.19					
Rieske$_{red}$[a]	2.74	2.30	2.35	2.12	2.30					
($S = 1/2$)		2.30	2.40	2.25	2.27					81.4

[a] Geometries of the reduced and the oxidized states are obtained with the lacvp** basis set instead of the lacvp basis set used throughout the paper. [b] The broken symmetry correction is not included.

and calculations, each iron atom is considered to be in the high spin state ($S = 5/2$ for Fe^{III} and $S = 2$ for Fe^{II}) and the spins on the two metals are antiferromagnetically coupled.[15,40−42] In the case of the smallest model I, ferromagnetic coupling was also investigated.

Small Model. The simplest model system of the Rieske cluster (I, Figure 4) contains only the first coordination sphere of the two iron atoms. Relevant bond distances and spin populations for the oxidized and reduced clusters with antiferromagnetic couplings are shown in Table 1. This table also reports a comparison between geometries optimized with a larger basis set (lacvp**) than the standard one (lacvp). Structural parameters are only slightly changed by the inclusion of polarization functions in the geometry optimizations, and more importantly, the computed IP is not significantly affected: 82.4 and 81.4 kcal/mol are the two values obtained from the two sets of geometries.

The values summarized in Table 1 indicate that the Fe−Fe distance is shortened upon one-electron reduction as also observed in previous calculations on [2Fe−2S] clusters.[40,41] Furthermore, reduction of the [2Fe−2S] cluster is associated with only a small decrease of the spin population of the iron atom with the lower formal oxidation state (i.e., iron coordinated by the two histidines). On the other hand, the spin populations on sulfur are significantly affected by the redox process, indicating that most of the added electron density is redistributed to these centers. In the reduced state, the spin populations of the sulfur atoms belonging to the cysteines have the same signs as the spin populations of the other two sulfur atoms; in the oxidized state the signs are instead opposite.

TABLE 2: Corrections to the IP in the Gas Phase (IP$_g$) of Rieske Cluster I (Δs = Solvent Effects, Δz = Zero-Point Effects, ΔBS = Broken Symmetry)

		IP$_g$		
		$+\Delta s$	$+\Delta s + \Delta z$	$+\Delta s + \Delta z + \Delta$BS[a]
IP (kcal mol^{-1}), $\epsilon = 4$	49.7	82.4	83.4	82.5

[a] The computed J_{ox} and J_{red} are 263 and 179 cm^{-1}.

The evaluation of the ionization potential was improved, adding the zero-point effects and the correction due to the spin contamination, the latter indicated as the "broken symmetry" correction. Table 2, where all the corrections are reported, shows that the broken symmetry correction is almost canceled by the zero-point effects, and both corrections are rather small. As a general extension of this result, the IP values of the other models, namely, II, III, IV, and V, for the Rieske cluster neglect the zero-point and the broken symmetry corrections.

An attempt was made to obtain the reduced cluster having the reduced iron ion coordinated by the cysteines. This structure (see table in the Supporting Information) was estimated to be about 10 kcal/mol less stable than the reduced state reported in

TABLE 3: Relevant Bond Distances and Spin Populations for the Small Model I of the Rieske Cluster with Ferromagnetic Coupling

	distance to Fe1 (Å)			distance to Fe2 (Å)		spin				
	Fe2	S1 S2	S3 S4	N1 N2	S1 S2	Fe1	Fe2	S1 S2	S3 S4	ΔE^a (kcal mol^{-1})
$Rieske_{ox}$	3.05	2.42	2.32	2.10	2.38	3.65	3.65	0.84	0.36	11.0
($S = 5$)		2.36	2.36	2.12	2.34			0.85	0.49	
$Rieske_{red}$	2.61	2.39	2.39	2.09	2.36	3.67	3.57	0.57	0.26	6.0
($S = {}^9/_2$)		2.39	2.42	2.13	2.36			0.58	0.23	

[a] The energy splitting (ΔE) with respect to the corresponding antiferromagnetic low-spin ground state is reported. Energy differences also include the broken symmetry and the zero-point corrections.

Table 1, confirming previous findings derived from an analogous system.[41]

The reduced and oxidized clusters with ferromagnetic coupling lie at higher energies than the corresponding antiferromagnetic states. The oxidized cluster with total spin $S = 5$ (ferromagnetic coupling) is 11.0 kcal/mol higher in energy than the corresponding low-spin state with $S = 0$ (antiferromagnetic coupling). In the case of the reduced state, the cluster with $S = {}^9/_2$ (ferromagnetic coupling) is 6.0 kcal/mol less stable than the cluster with $S = {}^1/_2$ (antiferromagnetic coupling). Table 3 summarizes relevant bond distances, spin populations and relative energies of the states with ferromagnetic coupling. This result confirms that the IP of the Rieske cluster has to be derived from the cluster with antiferromagnetic spin coupling.

Larger Models. The models for the Rieske cluster were extended by adding residues located in the outer coordination spheres, as shown in Figure 4. More specifically, the aspartate residue Asp205, which links the Rieske cluster and the mononuclear iron center was included in II. Addition of the carboxylate group changes the total charge of the oxidized state from 0 to −1. The effects of the total charge on the computed IP were tested with a model where Asp205 was considered protonated (III). According to the structural arrangement shown in Figure 2, neutrality of the model system can be achieved adding the negative aspartate together with a protonated histidine (IV), which mimics His208 coordinated to iron in the catalytic domain. For the latter model in the reduced form, geometry optimizations in the gas phase do not favor a charge separation between a carboxylate and a protonated imidazole ring, but the proton initially located on His208 tends to be transferred to Asp205. Therefore, the reduced form of the cluster was optimized constraining the N−H distance to the corresponding value obtained from the fully optimized oxidized cluster. A slightly different model with the neutral aspartic acid Asp205 hydrogen bonding to the unprotonated neutral His208 was also considered. For both the reduced and the oxidized clusters the latter arrangement gives slightly lower energies than IV (the computed energy differences are 1.9 and 1.4 kcal/mol for the reduced and the oxidized forms, respectively).

Table 4 summarizes the Fe−Fe distances of all the models investigated together with the computed IPs (the computed spin distribution for these models is almost identical to the one determined for the small model I). As already noted above, the Fe−Fe distance generally decreases upon one-electron reduction; however, this is not the case for II, where the Fe−Fe distances in the oxidized and reduced forms are identical; II differs from the other models because of its total charge. Inclusion of the negative residue Asp205 considerably lowers the corresponding computed IP (74.8 kcal/mol). This result can be interpreted in terms of the Coulomb repulsion between the reduced Rieske [2Fe−2S] cluster and the negative aspartate, which destabilizes the reduced form yielding a lower IP value. However, in the enzyme, the negative charge of Asp205 is balanced by the presence of the positively charged mononuclear iron(II) complex (the metal in the ferrous oxidation state is coordinated only by one charged ligand, Asp362). Indeed, the IP obtained from the model with Asp205 hydrogen bonding to a protonated histidine (IV) is comparable to the IP computed for the model without the negative residue (I).

TABLE 4: Fe−Fe Distances and IP Values for Structures I, II, III, IV, and V

	Fe1−Fe2 (Å)	IP (kcal mol^{-1})
$Rieske_{ox}$ I	2.86	
$Rieske_{red}$ I	2.75	82.4
$Rieske_{ox}$ II	2.85	
$Rieske_{red}$ II	2.85	74.8
$Rieske_{ox}$ III	2.82	
$Rieske_{red}$ III	2.76	84.5
$Rieske_{ox}$ IV[a]	2.88	
$Rieske_{red}$ IV[a]	2.83	84.0
$Rieske_{ox}$ IV[b]	2.91	
$Rieske_{red}$ IV[b]	2.82	84.6
$Rieske_{ox}$ V	2.88	
$Rieske_{red}$ V	2.82	81.9

[a] The negatively charged aspartate residue (Asp205) hydrogen bonds to protonated histidine His208. [b] The neutral aspartic acid residue (Asp205) hydrogen bonds to neutral histidine His208.

Model Including the Mononuclear Iron Center. An extended model of the Rieske cluster including the mononuclear iron center was employed to derive the IP value of the Rieske cluster (model V shown in Figure 5). The metal ion of the catalytic domain, which is in the ferrous state, is coordinated by the 2-His-1-carboxylate triad and a water molecule, hydrogen bonding to acetylamide, a model for Asn201. Asp205, joining the catalytic and the Rieske domains, is also included in the form of an acetate. The mononuclear iron(II) center is considered in the high-spin state, which is typically the ground state for these types of complexes.[12,43] When the Rieske cluster is in the oxidized state, the total charge of the entire model is 0.

Relevant geometrical details are reported in Figure 5, which also highlights spin populations and thus the coupling of the unpaired electrons of the three metal centers (a total spin of $S = {}^3/_2$ and $S = 2$ characterizes the reduced and the oxidized models, respectively). The spin distribution on the Rieske cluster is very similar to the one found in the smaller models, whereas the computed spin population of the ferrous ion located in the catalytic domain is indicative of high-spin iron(II).[44] From Table 4 it can be noted that the computed IP (81.9 kcal/mol) of the Rieske cluster modeled with the extended system V compares rather well with the computed IPs obtained from the smaller neutral models (i.e., neutral in the oxidized state). The larger deviation from the negatively charged model II has already been addressed.

3.2. Mononuclear Iron(II) Center. Dioxygen activation in the catalytic domain of Rieske dioxygenases can be viewed as initiated by two processes: dioxygen binding to the mononuclear

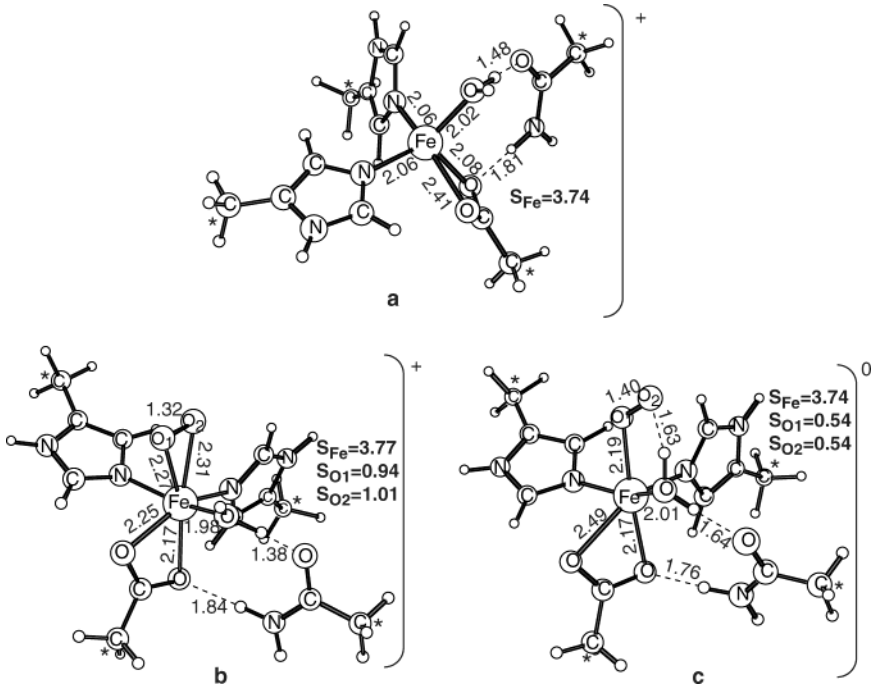

Figure 6. Small model for the mononuclear iron site: (a) iron(II) complex ($S = 2$); (b) dioxygen-bound iron(II) complex, $[Fe^{II}-O_2]^{2+}$ ($S = 3$); (c) reduced dioxygen-bound complex, $[Fe^{II}-O_2]^{+}$ ($S = {}^5/_2$). Relevant bond distances (Å) and spin populations are reported. The total charge is also shown.

iron(II) complex and one-electron transfer from the Rieske domain. These chemical events are investigated in this section with different models mimicking the mononuclear $[Fe^{II}-O_2]^{2+}$ and $[Fe^{II}-O_2]^{+}$ species. Iron is always considered in the high spin state, which is a quintet ($S = 2$) without bound dioxygen.[12] Geometries of $[Fe^{II}-O_2]^{2+}$ were optimized for the septet state ($S = 3$), which was previously found to be the ground state.[19,45] For $[Fe^{II}-O_2]^{+}$ only the sextet state ($S = {}^5/_2$) with the unpaired d-electrons of iron ferromagnetically coupled to the unpaired spin density on O_2 is investigated. In the previous study on naphthalene dioxygenase, we found that the quartet and the sextet states of the $[Fe^{II}-O_2]^{+}$ species have similar energies.[19] The electron affinity of $[Fe^{III}-OOH]^{2+}$ yielding $[Fe^{II}-OOH]^{+}$ was also explored again for the high-spin states, $S = {}^5/_2$ and $S = 2$, respectively. The rigidity of the protein backbone was taken into account by freezing some atoms according to the X-ray crystal structures.[7,14]

Small Model for the Dioxygen-Bound Iron Complex. The smallest model for the mononuclear center is depicted in Figure 6a, where iron is coordinated by a water ligand and by the 2His-1-carboxylate facial triad. With the carboxylate binding in a bidentate fashion, the metal has a distorted octahedral coordination with a missing ligand. Asn201 located in the second coordination sphere was also included.

Crystal structures of dioxygen trapped in the catalytic domain show O_2 bound side-on to iron in place of the water ligand.[7,14] Because the X-ray analysis did not detect any water in the first coordination sphere of the metal, the water ligand has to be displaced either before or after dioxygen binding. Water is computed to be tightly bound to the iron complex of Figure 6 and geometry optimizations of the metal complex with water initially placed in the second coordination sphere always yielded water bound to iron. However, by freezing the water/iron distance to 5 Å, it is estimated that displacement of the water from the metal first coordination sphere costs 14 kcal/mol. It follows that dissociation of water at this stage of the reaction is unlikely. Furthermore, the subsequent reaction step, namely, dioxygen binding, does not lead to any energy gain to balance the energy loss due to water dissociation. Binding of dioxygen to the high-spin iron(II) complex with water placed in the second coordination sphere is estimated to be a nearly thermoneutral process, which would become endergonic when the entropy loss of free O_2 is included. Under these circumstances the water ligand was maintained in the modeling of dioxygen activation described below.

With the water still in the first coordination sphere, binding of O_2 to iron in a side-on fashion was calculated to be endothermic by 1.8 kcal/mol. The corresponding end-on structure was not considered in detail because O_2 tended to dissociate from the metal. Figure 6b reports the structure of the $[Fe^{II}-O_2]^{2+}$ species together with the corresponding spin distribution. The computed spin populations on iron is 3.77, indicating that iron remains in the ferrous oxidation state and it is not capable to reduce dioxygen to superoxide. The free energy change associated with dioxygen binding was properly computed after releasing the frozen coordinates of the model system of Figure 6a,b. From the reoptimized geometries, dioxygen binding was found to be endergonic by 11.5 kcal/mol mainly because of the entropic contribution $-T\Delta S$ of 11.0 kcal/mol.

Small Model for the Electron Transfer. The electron transfer to the mononuclear iron(II) complex can in principle occur before O_2 binds to the metal, and thus the electron affinity of the complex depicted in Figure 6a was evaluated. The one-electron transfer to Fe^{II} yields the unstable Fe^{I} species, and the computed electron affinity is therefore rather low, 52.4 kcal/mol. Furthermore, it has to be noted that the Fe^{II} complex is positively charged, and it becomes neutral upon one-electron reduction. As discussed before for the Rieske cluster, a negative residue, as Asp205 not included in the actual model structure, might significantly decrease the computed EA. Because of the very low computed EA (52.4 kcal/mol) of the mononuclear iron(II) center in the resting state and because of the higher IP (72−84 kcal/mol) of the reduced Rieske cluster, the one-electron transfer before dioxygen binding can be safely excluded.

Reduction of $[Fe^{II}-O_2]^{2+}$ to $[Fe^{II}-O_2]^{+}$ was then investigated by adding one electron to dioxygen bound to iron(II). We found

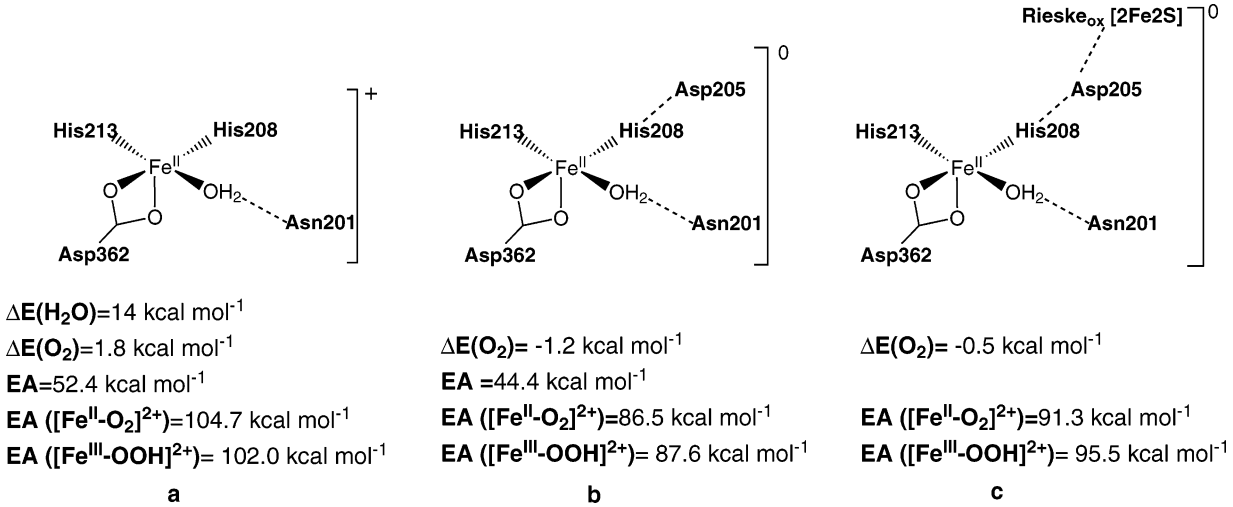

Figure 7. Summary of the computed properties for the mononuclear iron complex modeled in three different ways: (a) small model of Figure 6; (b) larger model including aspartate Asp205; (c) big model including the oxidized Rieske cluster.

that the best arrangement of the reduced form is the end-on binding mode depicted in Figure 6c, where the water ligand interacts with bound O_2 through a strong hydrogen bond. The computed spin population on the metal ($S = 3.74$) is indicative of iron(II),[44] whereas the total spin population on dioxygen ($S = 1.08$) reflects the radical character of the superoxide. The side-on arrangement was also considered (see figure in the Supporting Information) but found to lie 4.5 kcal/mol higher in energy. The side-on complex center lacks the extra stabilization due to the strong hydrogen bond between the superoxide and the water ligand. The computed EA of $[Fe^{II}-O_2]^{2+}$ (104.7 kcal/mol) is reported in Figure 7a together with a summary of all the other computed properties for the mononuclear iron center.

Once one electron is transferred from the Rieske cluster yielding $[Fe^{II}-O_2]^{+}$, a proton can be supplied by an external proton donor to the mononuclear center forming the iron(III)−hydroperoxo complex. Because suitable residues acting as proton donors were not identified, the proton transfer process was not investigated and a proton was simply added to $[Fe^{II}-O_2]^{+}$ (see the optimized geometry of $[Fe^{III}-OOH]^{2+}$ in the Supporting Information) and its EA computed. Importantly, the EA of the ferric−hydroperoxo intermediate controls the transfer of the second external electron from the Rieske domain. Within the accuracy of the present computational approach, the calculated EA of $[Fe^{III}-OOH]^{2+}$ (102.0 kcal/mol; see Figure 7) is rather similar to the EA for $[Fe^{II}-O_2]^{2+}$ (104.7 kcal/mol). Although the computed IPs and EAs appear strongly dependent on the total charge of the model, the comparison is fairly safe because $[Fe^{III}-OOH]^{2+}$ and $[Fe^{II}-OOH]^{+}$ have the same total charge as $[Fe^{II}-O_2]^{2+}$ and $[Fe^{II}-O_2]^{+}$, respectively. It was already noted that charged residues located in the outer coordination spheres might affect computed EAs or IPs, and thus other models for the mononuclear iron center needed to be explored.

Larger Models for the Electron Transfer. Electron affinities for $[Fe^{II}-O_2]^{2+}$ and $[Fe^{III}-OOH]^{2+}$ were also evaluated with the models depicted in Figure 8. The small model of Figure 6 is first enlarged adding a carboxylate group in the metal second coordination sphere to mimic Asp205 (Figure 8a), and therefore, the total charge changes from +1 to 0. Resembling the structure previously reported in Figure 5, a larger model including the Rieske cluster was also employed to compute the EA for $[Fe^{II}-O_2]^{2+}$. In this case, the wave function corresponding to the reduced Rieske cluster and $[Fe^{II}-O_2]^{2+}$ could not be obtained because the Rieske cluster is readily oxidized by the

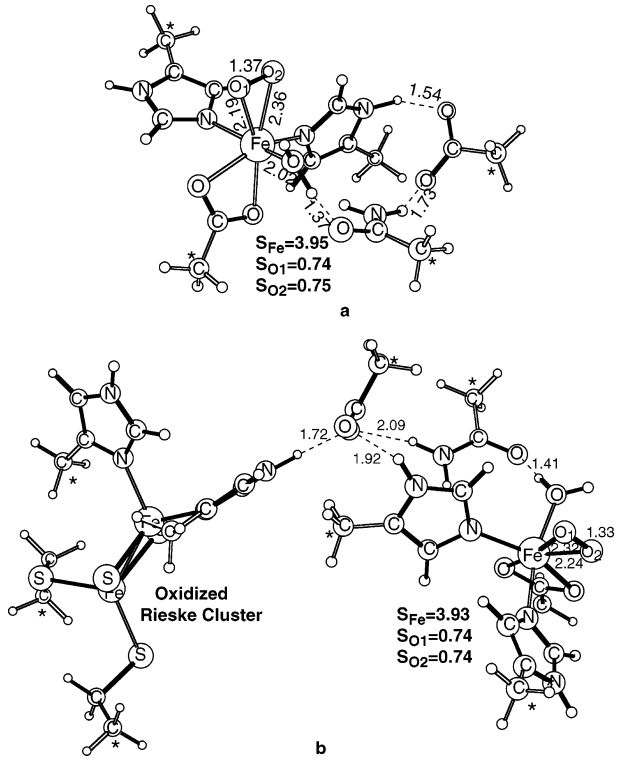

Figure 8. Two larger models for the mononuclear iron site; the dioxygen-bound iron(II) species is shown, $[Fe^{II}-O_2]^{2+}$. (a) The model includes Asp205 in the metal second coordination sphere ($S = 3$). (b) The model includes the adjacent Rieske cluster in the oxidized state (the total spin is still $S = 3$). Relevant bond distances (Å) and spin populations are reported.

dioxygen-bound iron complex generating the $[Fe^{II}-O_2]^{+}$ species. Therefore, the EA of the mononuclear center with the large model was evaluated with the Rieske cluster always in the oxidized state. Concerning the total charge, the large model shown in Figure 8b is neutral when oxidized and negatively charged when reduced.

It was first verified that the binding energy of molecular oxygen to Fe^{II} was not significantly affected by the extension of the model and the three values obtained for three different models are gathered in Figure 7. The calculations indicate that the larger models of Figure 8 favor dioxygen binding by 2.3−3.0 kcal/mol with respect to the smaller model of Figure 6. The inclusion of the carboxylate group of Asp205 in the metal

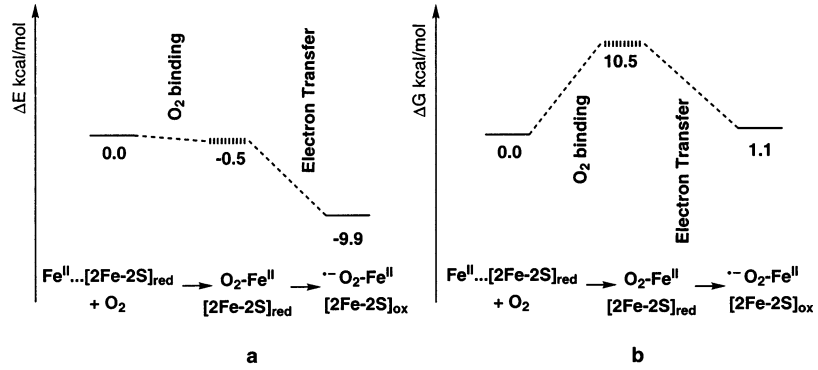

Figure 9. Energy profile corresponding to the two-step dioxygen activation: O_2 binding at the mononuclear iron center and electron transfer from the reduced Rieske cluster. (a) The computed energies without any thermal correction are reported as obtained from the big model including both the metal centers. (b) The profile has been corrected for the entropic contribution ($-T\Delta S = 11.0$ kcal/mol) obtained from smaller models. It is assumed that the only significant entropy contribution derives from the O_2-binding step.

second coordination sphere provides a rationale for this behavior as already noted in the case of dioxygen binding to hemerythrin, a binuclear non-heme iron enzyme.[46] The negative group stabilizes the dioxygen-bound complex, which can also formally be described as a ferric−superoxo species. In contrast to the small effects on the computed binding energy of O_2, the enlargement of the model affects the computed electron affinity significantly. Inspection of the summary reported in Figure 7 indicates that the smallest model, where the carboxylate group of Asp205 is not included, gives the highest EA of $[Fe^{II}-O_2]^{+1}$ (104.7 kcal/mol). Addition of this negative residue in the second coordination sphere considerably lowers the computed EA (86.5−91.3 kcal/mol). Similarly, the different structures provide different values for the electron affinity of the protonated species, namely the $[Fe^{III}-OOH]^{2+}$ complex. Nevertheless, for all the three models the computed EA of the ferric−hydroperoxo intermediate can be considered similar to the electron affinity of the $[Fe^{II}-O_2]^{2+}$ species.

3.3. Dioxygen Activation. With the model including both the Rieske and the mononuclear centers (see Figures 5 and 8b) the energy difference for the following reaction has been calculated:

$$\{\text{Rieske}_{red} + Fe^{2+}\} + O_2 \rightarrow \{\text{Rieske}_{ox} + [Fe^{II}-O_2]^{+}\} \qquad \Delta E = -9.9 \text{ kcal/mol} \quad \text{(A)}$$

The reactant comprises free O_2 and the reduced Rieske cluster linked to the mononuclear iron(II) center. It was already mentioned that it was impossible to converge the wave function of the big model having simultaneously the Rieske cluster in the reduced state and the $[Fe^{II}-O_2]^{2+}$ species. As soon as dioxygen approaches the metal in the catalytic domain, it is reduced by the Rieske cluster leading to a superoxo-bound iron(II) complex, and this chemical transformation is computed to be exothermic by 9.9 kcal/mol. It has to be noted that the investigation of this process does not implicate addition of any external electron, because all the reducing equivalents are included in the model.

The computed energy change for reaction A can be decomposed into two different parts: the small energy gain associated with O_2 binding to iron(II) (−0.5 kcal/mol, Figure 7) and the energy change associated with the electron-transfer step:

$$\text{Rieske}_{red} + [Fe^{II}-O_2]^{2+} \rightarrow \text{Rieske}_{ox} + [Fe^{II}-O_2]^{+} \quad \text{(B)}$$

The latter energy contribution corresponds to the difference between the computed IP of the reduced Rieske cluster and the EA of $[Fe^{II}-O_2]^{2+}$. With the large model, this energy difference is 9.4 kcal/mol, which is close to $\Delta E = -9.9$ kcal/mol due to the near-zero binding energy of O_2. The energy profile of Figure 9a summarizes the energy changes arising from the O_2-binding step and the electron-transfer process as derived from the big model. The overall reaction is computed to be exothermic because the electron affinity of $[Fe^{II}-O_2]^{2+}$ is larger than the ionization potential of the reduced Rieske cluster and consequently, the O_2-binding step can be regarded as the trigger for the electron-transfer process. Although the evaluations of the IP and the EA are rather sensitive to the charged residues included in the model, this trend (i.e., the IP of the Rieske cluster being lower than the EA of the dioxygen-bound iron(II) complex) is observed for all the models investigated, as derived from the comparison of Table 4 and Figure 7. It is interesting to note that the difference between the IP and the EA taken from the small models including in both cases the aspartate residue Asp205 is very similar to the corresponding difference derived from the large model including both metal centers: the IP of the Rieske cluster II of Figure 4 is 74.8 kcal/mol and the EA of the mononuclear complex shown in Figure 8a is 86.5 kcal/mol, leading to a difference of 11.7 kcal/mol, reasonably close to 9.4 kcal/mol obtained for the large model.

Although the computed energy difference for reaction A does not include any thermal effects, a free energy diagram may be obtained for the dioxygen activation process assuming that the major correction arises from the entropy loss ($T\Delta S$) associated with the O_2-binding step. From the small model for the mononuclear iron complex (Figure 6), an entropic contribution ($-T\Delta S$) of 11.0 kcal/mol was derived, which can be used to construct the free energy diagram shown in Figure 9b. Importantly, the entropy loss is almost balanced by the exothermicity of the electron transfer, which makes dioxygen activation only slightly endergonic by 1.1 kcal/mol. Within the accuracy of the present calculations, the computed energy change for this process suggests that the product is not largely favored over the reactant. The tendency of the overall enzymatic reaction to ultimately proceed toward naphthalene dioxygenation will be determined by the subsequent steps of the catalytic cycle. The specific enzymatic environment might be relevant in tuning the extent to which the dioxygen-bound species is formed as an iron(II)−superoxo complex. There might be effects from the protein environment contributing to stabilize the superoxo iron complex as for the oxy form of hemerythrin and these effects would increase the computed exergonicity of the reaction. On the other hand, it has to be noted that a higher dielectric constant

for the description of the long-range solvent effects would increase the computed endergonicity.

Electron Transfer between the Rieske Cluster and the Mononuclear Center. On the basis of the model system including both the Rieske cluster and the mononuclear iron site, the rate constant for the electron transfer between the two metal centers was estimated using the equations described in the computational details. The distance d (8.73 Å) between the sites was obtained from the optimized structure of the large model with the reduced Rieske cluster. From the reorganization energy λ (23.2 kcal/mol) obtained as described in the computational details and from the ET driving force ($\Delta G = -9.4$ kcal/mol) discussed above, an activation energy of only 1.9 kcal/mol is calculated, which indicates a very easy thermal activation for this ET process. As regards the β parameter, the Beratan and Onuchic approach was employed to calculate the decay coupling for three intuitive ET pathways leading from the Rieske cluster to the mononuclear site.[36,38,39] Although in the more rigorous approach a program finding the most efficient ET pathways would be used,[39] it is believed that the system studied is simple enough to allow for visual selection of the most probable ET pathways. Three pathways connecting Fe2 and Fe3 were selected, all of them passing through Asp205, which links the Rieske cluster to the catalytic site; one pathway continues through His208 to Fe3, whereas the other two pathways reach Fe3 either through Asn201 and the water ligand or through Asn201 and His208 (see Figure 5) Their corresponding decay couplings range between 3.6×10^{-3} and 5.2×10^{-3}; from the calculated decay coupling of 5.2×10^{-3} and the distance between the sites, the β value was evaluated, and it is equal to $\beta = 1.4$ Å^{-1}, which falls into the range of commonly observed values for proteins.[37,47] Finally, the computed k_{ET} was 2.2×10^6 s^{-1}, which indicates a very fast ET between the Rieske cluster and the catalytic site.

3.4. Binding of NO to Iron(II). Nitric oxide (NO) is often used as surrogate for O_2 to acquire information on the enzyme active site in the absence of turnovers. Therefore, it is interesting to compare the properties of the $Fe^{II}-O_2$ and the $Fe^{II}-NO$ complexes. In the case of naphthalene 1,2-dioxygenenase, signals of a nitrosyl adduct arise in the EPR spectra of resting NDO (resting NDO contains the oxidized Rieske cluster and the Fe^{II} mononuclear center) upon exposure to NO.[16] Under exposure of O_2 no corresponding dioxygen-bound complexes were detected. In analogy to the investigation performed for $[Fe^{II}O_2]^{2+}$, the binding energy of NO to Fe^{2+} was computed using different models: the large model shown in Figure 8b and two smaller models including only the mononuclear iron-(II) site (Figures 6b and 8a); side-on O_2 of these models was replaced with NO binding to iron(II) in an end-on fashion. The iron(II)−NO adduct is considered in the quartet spin state ($S = {}^3/_2$), which corresponds to the four unpaired d-electrons of Fe^{II} antiferromagnetically coupled to the unpaired electron localized on NO. As in the case of O_2 binding, the water ligand is maintained in the first coordination sphere of the iron complex. In all the models examined, nitric oxide tends to bind stronger to Fe^{II} than O_2 by approximately 6 kcal/mol. In particular, if the entropic term $T\Delta S$ is not included, the large model of Figure 8b predicts that NO has an enthalpic binding energy to iron(II) of 6.5 kcal/mol as compared to a corresponding enthalpic binding energy of only 0.5 kcal/mol for O_2 (Figure 7c).

Employing the same large model, it has been probed whether the NO adduct is able to trigger the one-electron transfer from the reduced Rieske cluster, as has been proposed above for the dioxygen activation process. Addition of one electron to $[Fe^{II}-NO]^{2+}$ leads to a triplet ground state ($S = 1$) for the mononuclear center, where the metal can be considered to be in the ferrous oxidation state and two unpaired electrons are located on the NO-ligand (the corresponding spin distribution is: Spin(Fe) = 3.59 and Spin(NO) = −1.89). By means of calculations similar to those performed for $Fe^{II}-O_2$ and reported in Figure 9a, the $Fe^{II}-NO$ state where the electron remains on the reduced Rieske cluster is found to be more stable by 2.7 kcal/mol than the corresponding species where Fe−NO is reduced by one electron and the Rieske cluster is oxidized. This result suggests that reduction of the nitrosyl adduct is not a favorable process, in contrast to the dioxygen case, where the one-electron reduction was required to stabilize the dioxygen-bound iron complex. Therefore, formation of a nitrosyl adduct is not likely to involve any electron transfer from the reduced Rieske cluster.

Hence, the calculations discussed above lead to the conclusions that NO might bind to the Fe^{II} iron site independently on the oxidation state of the Rieske cluster and the adduct is formed if the enthalpic binding energy of NO to Fe^{II} balances the entropy loss due to the trapping of free NO. With a small model having all the coordinates released, the entropy term was evaluated to be $-T\Delta S = 11.6$ kcal/mol with respect to free NO, indicating that NO is unbound by about 5 kcal/mol ($\Delta H = -6.5$ kcal/mol, $\Delta G = 5.1$ kcal/mol) at the free energy level. Consequently, the formation of the nitrosyl adduct detected by EPR spectroscopy[16] and X-ray crystallography[7] is explained by the present computational approach if an error of 6−8 kcal/mol affects the computed free energy, that is, the calculation of the enthalpy as well as the evaluation of the entropy. This is a larger error than expected using B3LYP, but it cannot be ruled out. Importantly, the computed binding energy of O_2 is about 6 kcal/mol lower than that of NO, and the different binding energies of the two small molecules to Fe^{II} should account for the experimental indication that a dioxygen-bound iron complex is not detected when the Rieske cluster is in the oxidized state.[16]

4. Summary and Conclusions

Using different models to mimic the active site of naphthalene 1,2-dioxygenase the mechanism of dioxygen activation by Rieske-type dioxygenases was explored. The free energy diagram depicted in Figure 9 could be derived from energy differences computed from the largest model comprising the two metal centers located in the catalytic and Rieske domains (see Figure 5). The computed binding energy of dioxygen to iron(II) was found not to be sufficient to balance the entropy loss associated with the trapping of free O_2. With a computed endergonicity of 10.5 kcal/mol, an oxygen-bound iron(II) complex is not expected to be a stable intermediate that can be experimentally observed. However, when an electron is available at the neighboring Rieske cluster, the calculations show that the electron transfer process from the Rieske domain to the oxygen-bound complex is exothermic by 9.4 kcal/mol. This means that the electron affinity of the mononuclear center becomes higher than the ionization potential of the Rieske cluster as soon as dioxygen enters the first coordination sphere of iron. Assuming that the entropy change associated with the ET step is negligible, the free energy change for the overall reaction (i.e., dioxygen binding coupled to the redox process) is 1.1 kcal/mol. Interestingly, the exothermicity of the electron transfer step is almost canceled by the entropy loss associated with the preceding dioxygen binding process. Therefore, the electron transfer is crucial to lower the energetics of dioxygen activation and it leads to an iron(II)−superoxo species. The computed free energy change together with the estimate of a low activation

barrier for the electron transfer process suggests that the first step of dioxygen activation is a reversible equilibrium, which can be finely shifted toward the reactant or the product sides by an appropriate protein environment. After protonation, the subsequent ferric−hydroperoxo complex might be able to carry out naphthalene dioxygenation, as suggested by experiments and theoretical calculations.[16,19]

The catalytic cycle of naphthalene dioxygenase (see Figure 3) implies that a second external electron is provided by NADH. The observations from single turnover experiments suggest that the second external electron is not necessary for dioxygen activation and that it can be supplied at a later stage of catalysis (after substrate oxidation).[16] If the second electron can enter the catalytic cycle at an earlier stage, $[Fe^{II}-OOH]^{+}$ could be formed. Our DFT calculations indicate that the electron affinity of the ferric−hydroperoxo species (see Figure 7) is comparable to the one of the iron(II)$-O_2$ complex. Similarly to the reduction of $[Fe^{II}-O_2]^{2+}$ by the Rieske cluster, which was estimated to be exothermic, the formation of $[Fe^{II}-OOH]^{2+}$ from $[Fe^{III}-OOH]^{2+}$ is also thermodynamically favored if the second external electron is available at the Rieske cluster.

Acknowledgment. We thank Dr. Andreas Karlsson and Prof. Hans Eklund (Uppsala University, Sweden) for providing essential information on the structure. We gratefully acknowledge the National Supercomputer Center (Sweden) for generous grants of computer time at the SGI3800 and MONOLITH.

Supporting Information Available: Table of the electronic configuration of the Rieske cluster and figures of the $[Fe-O_2]^{+}$ species and ferric and ferrous hydroperoxo species. This material is available free of charge via the Internet at http://pubs.acs.org.

References and Notes

(1) Gibson, D. T.; Parales, R. E. *Curr. Opin. Biotechnol.* **2000**, *11*, 235−243.
(2) Jeffrey, A. M.; Yeh H, J. C.; Jerina, D. M.; Patel, T. R.; Davey, J. F.; Gibson, D. T. *Biochemistry* **1975**, *14*, 575−584.
(3) Kauppi, B.; Lee, K.; Carredano, E.; Parales, R. E.; Gibson, D. T.; Eklund, H.; Ramaswamy, S. *Structure* **1998**, *6*, 571−586.
(4) Parales, R. E. *J. Ind. Microbiol. Biotechnol.* **2003**, *30*, 271−273.
(5) Ramaswamy, S. In *Handbook of Metalloproteins*; Messerschmidt, A., Huber, R., Poulos, T., Wieghardt, K., Eds.; John Wiley & Sons: Chichister, U.K., 2001; pp 613−621.
(6) Nordlund, P. In *Handbook of metalloproteins*; Bertini, I., Sigel, A., Sigel, H., Eds.; Marcel Dekker: New York, 2001; pp 511−517.
(7) Karlsson, A. Ph.D. thesis, Swedish University of Agricultural Science, Uppsala, **2002**.
(8) Bugg, T. D. H. *Tetrahedron* **2003**, *59*, 7075−7101.
(9) Hegg, E. L.; Que, L., Jr. *Eur. J. Biochem.* **1997**, *250*, 625−629.
(10) Que, L., Jr. *Nature Struct. Biol.* **2000**, *7*, 182−184.
(11) Costas, M.; Mehn, M. P.; Jensen, M. P.; Que, L., Jr. *Chem. Rev.* **2004**, *104*, 939−986.
(12) Solomon, E. I.; Brunold, T. C.; Davis, M. I.; Kemseley, J. N.; Lee, S.-K.; Lehnert, N.; Neese, F.; Skulan, A. J.; Yang, Y.-S.; Zhou, J. *Chem. Rev.* **2000**, *100*, 235−349.
(13) Ryle, M. J.; Hausinger, R. P. *Curr. Opin. Chem. Biol.* **2002**, *6*, 193−201.
(14) Karlsson, A.; Parales, J. V.; Parales, R. E.; Gibson, D. T.; Eklund, H.; Ramaswamy, S. *Science* **2003**, *299*, 1039−1042.
(15) Holm, R.; Kennepohl, P.; Solomon, E. I. *Chem. Rev.* **1996**, *96*, 2239−2314.
(16) Wolfe, M. D.; Parales, J. V.; Gibson, D. T.; Lipscomb, J. D. *J. Biol. Chem.* **2001**, *276*, 1945−1953.
(17) Wolfe, M. D.; Lipscomb, J. D. *J. Biol. Chem.* **2001**, *278*, 829−835.
(18) Lee, K. *J. Bacter.* **1999**, *181*, 2719−2725.
(19) Bassan, A.; Blomberg, M. R. A.; Siegbahn, P. E. M. *J. Biol. Inorg. Chem.* **2004**, *9*, 439−452.
(20) Becke, A. D. *J. Chem. Phys.* **1993**, *98*, 5648−5652.
(21) Stevens, P. J.; Devlin, F. J.; Chablowski, C. F.; Frisch, M. J. *J. Phys. Chem.* **1994**, *98*, 11623−11627.
(22) Lee, C.; Yang, W.; Parr, R. G. *Phys. Rev. B* **1988**, *37*, 785−789.
(23) Jaguar 4.0. Schrödinger, Inc., Portland, Oregon, **2000**.
(24) Frisch, M. J.; Trucks, G. W.; Schlegel, H. B.; Scuseria, G. E.; Robb, M. A.; Cheeseman, J. R.; Zakrzewski, V. G.; Montgomery, J. A., Jr.; Stratmann, R. E.; Burant, J. C.; Dapprich, S.; Millan, J. M.; Daniels, A. D.; Kudin, K. N.; Strain, M. C.; Farkas, O.; Tomasi, J.; Barone, V.; Cossi, M.; Cammi, R.; Mennucci, B.; Pomelli, C.; Adamo, C.; Clifford, S.; Ochterski, J.; Petersson, G. A.; Ayala, P. Y.; Cui, Q.; Morokuma, K.; Malick, D. K.; Rabuck, A. D.; Raghavachari, K.; Foresman, J. B.; Cioslowski, J.; Ortiz, J. V.; Stefanov, B. B.; Liu, G.; Liashenko, A.; Piskorz, P.; Komaromi, I.; Gomperts, R.; Martin, R. L.; Fox, D. J.; Keith, T.; Al-Laham, M. A.; Peng, C. Y.; Nanayakkara, A.; Gonzalez, C.; Challacombe, M.; Gill, P. M. W.; Johnson, B.; Chen, W.; Wong, M. W.; Andres, J. L.; Head-Gordon, M.; Replogle, E. S.; Pople, J. A. *Gaussian98*; Gaussian Inc.: Pittsburgh, PA, 1998.
(25) Hay, P. J.; Wadt, W. R. *J. Chem. Phys.* **1985**, *82*, 299−310.
(26) Siegbahn, P. E. M. *J. Comput. Chem.* **2001**, *22*, 1634−1645.
(27) Siegbahn, P. E. M.; Blomberg, M. R. A. *Chem. Rev.* **2000**, *100*, 421−437.
(28) Tannor, D. J.; Marten, B.; Murphy, R.; Friesner, R. A.; Sitkoff, D.; Nicholls, A.; M., R.; Goddard III, W. A.; Honig, B. *J. Am. Chem. Soc.* **1994**, *116*, 11875−11882.
(29) Marten, B.; Kim, K.; Cortis, C.; Friesner, R. A.; Murphy, R. B.; Ringnalda, M.; Sitkoff, D.; Honig, B. *J. Biol. Chem.* **1996**, *100*, 11775−11788.
(30) Mouesca, J.-M.; Chen, J. C.; Noodleman, L.; Bashford, D.; Case, D. A. *J. Am. Chem. Soc.* **1994**, *116*, 11898−11914.
(31) Siegbahn, P. E. M. *Q. Rev. Biophys.* **2003**, *36*, 91−145.
(32) Curtiss, L. A.; Raghavachari, K.; Redfern, P. C.; Pople, J. A. *J. Chem. Phys.* **2000**, *112*, 7374−7383.
(33) Blomberg, M. R. A.; Siegbahn, P. E. M. *J. Phys. Chem. B* **2001**, *105*, 9375−9386.
(34) Siegbahn, P. E. M.; Blomberg, M. R. A. *Annu. Rev. Phys. Chem.* **1999**, *50*, 221−249.
(35) Marcus, R. A.; Sutin, N. *Biochim. Biophys. Acta* **1985**, *811*, 265−322.
(36) Beratan, D. N.; Onuchic, J. N.; Betts, J. N.; Bowler, B. E.; Gray, H. B. *J. Am. Chem. Soc.* **1990**, *112*, 7915−7921.
(37) Machonkin, T. E.; Solomon, E. I. *J. Am. Chem. Soc.* **2000**, *122*, 12547−12560.
(38) Beratan, D. N.; Betts, J. N.; Onuchic, J. N. *Science* **1991**, *252*, 1285−1288.
(39) Betts, J. N.; Beratan, D. N.; Onuchic, J. N. *J. Am. Chem. Soc.* **1992**, *114*, 4043−4046.
(40) Sigfridsson, E.; Olsson, M. H. M.; Ryde, U. *Inorg. Chem.* **2001**, *40*, 2509−2519.
(41) Ullmann, G. M.; Noodleman, L.; Case, D. A. *J. Biol. Inorg. Chem.* **2002**, *7*, 632−639.
(42) Noodleman, L.; Pend, C. Y.; Case, D. A.; Mouesca, J.-M. *Coordin. Chem. Rev.* **1995**, *144*, 199−244.
(43) Solomon, E. I. *Inorg. Chem.* **2001**, *40*, 3656−3669.
(44) It has to be noted that for high spin iron complexes the computed spin population on the metal does not strictly correspond to the number of d-electrons as expected from the oxidation state. With the coordination environment dominated by oxygen and nitrogen ligands the computed spin population on high-spin Fe^{II} ($S = 2$) is usually 3.7−3.8 and about 4.0−4.1 for high-spin Fe^{III} ($S = {}^5/_2$).
(45) Bassan, A.; Blomberg, M. R. A.; Siegbahn, P. E. M. *Chem. Eur. J.* **2003**, *9*, 106−115.
(46) Wirstam, M.; Lippard, S. J.; Friesner, R. A. *J. Am. Chem. Soc.* **2003**, *125*, 3980−3987.
(47) Barbara, P. F.; Meyer, T. J.; Ratner, M. A. *J. Phys. Chem.* **1996**, *100*, 13148−13168.
(48) Bassan, A. Ph.D. thesis, Stockholm University, Stockholm, 2004.